Two-Dimensional Chemiresistive Covalent Organic Framework with High Intrinsic Conductivity

Zheng Meng,[1] Robert M. Stolz,[1] Katherine A. Mirica*[1]

[1]Department of Chemistry, Burke Laboratory, Dartmouth College, Hanover, New Hampshire, 03755

Supporting Information Placeholder

ABSTRACT: This paper describes the synthesis of a novel intrinsically conductive two-dimensional (2D) covalent organic framework (COF) through the aromatic annulation of 2,3,9,10,16,17,23,24-octa-aminophthalocyanine nickel(II) and pyrene-4,5,9,10-tetraone. The intrinsic bulk conductivity of the COF material (termed **COF-DC-8**) reached 2.51×10^{-3} S/m, and increased by three orders of magnitude with I_2 doping. Electronic calculations revealed an anisotropic band structure, with the possibility for significant contribution from out-of-plane charge-transport to the intrinsic bulk conductivity. Upon integration into chemiresistive devices, this conductive COF showed excellent responses to various reducing and oxidizing gases, including NH_3, H_2S, NO, and NO_2, with parts-per-billion (ppb) level of limits of detection (LOD for NH_3=70 ppb, for H_2S=204 ppb, for NO=5 ppb, and for NO_2=16 ppb based on 1.5 min exposure). Electron paramagnetic resonance spectroscopy and X-ray photoelectron spectroscopy studies suggested that the chemiresistive response of the **COF-DC-8** involves charge transfer interactions between the analyte and nickelphthalocyanine component of the framework.

INTRODUCTION

The development of chemically robust, porous, and electrically conductive nanomaterials drives progress in electronic devices,[1] energy storage,[2] catalysis,[3] and chemical sensing.[4] Recent advances in the synthesis of electrically conductive metal−organic frameworks (MOFs) have enabled a range of applications in electrocatalysis, energy storage, and chemical sensing that were previously inaccessible using traditionally insulating MOFs.[5] Both through-bond and through-space charge transport mechanisms have proven to be effective in promoting conductivity in MOFs.[5] In particular, the molecular design strategy focusing on planar two-dimensional MOFs, in which the formation of π–d conjugated sheets can promote the delocalization of charge, has yielded metallic conductivities.[6] Despite progress in the development of conductive MOFs, the design and synthesis of electrically conductive π–conjugated covalent organic frameworks (COFs) connected by chemically robust bonds—which arguably possess superior chemical stability to frameworks derived from reversible coordination chemistry and borate or Schiff-base chemistry —has remained a tremendous challenge.[7] Although doping of COFs with oxidants and guest molecules has led to conductivities of ~10^{-2} to 10^{-1} S/m,[8] access to intrinsically conductive COFs with high bulk conductivity remains limited.[9]

Capitalizing on the general principles of molecular engineering for other classes of conductive materials (e.g., conductive organic polymers,[10] conductive organic molecular solids,[11] and conductive coordination polymers),[5b, 5c, 12] the strategy for maximizing the intrinsic bulk conductivity of COFs can leverage through-bond and through-space charge transport characteristics. To achieve through-bond charge transport, the covalent linkages formed during COF synthesis must promote efficient charge delocalization. Previous studies on 1D and 2D conjugated polymers with single bonds in their backbones rarely showed high charge carrier mobility values,[13] suggesting that borate

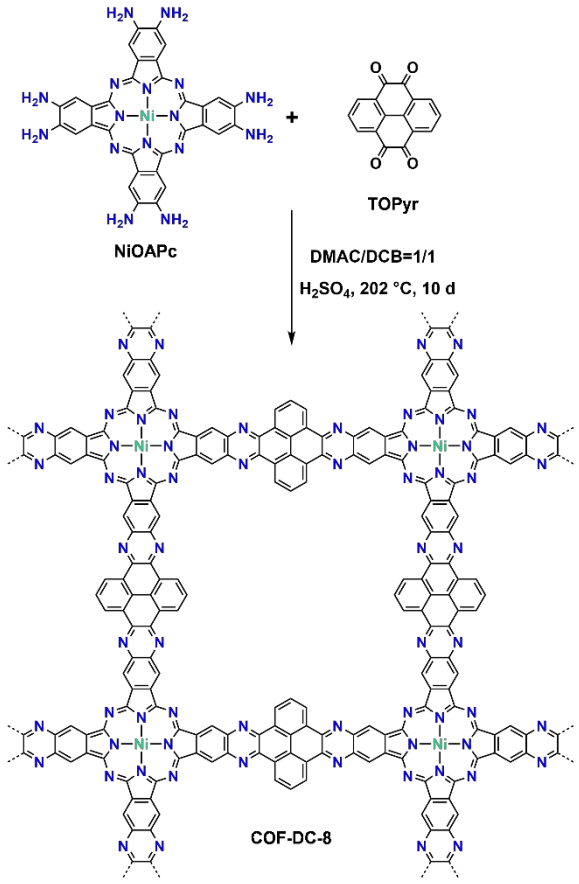

Scheme 1. The synthetic route for 2D conductive **COF-DC-8** with nickelphthalocyanine and pyrene subunits connected by pyrazine rings.

and imine linkages in typical COFs may be inefficient at facilitating through-bond charge transport. While full annulation of building blocks through aromatic linkages has been established as a promising strategy for conjugated 2D COF formation,[7e, 13c, 14] it has not yet yielded materials with high intrinsic conductivities. Interestingly, recent studies highlighted the unique role of topology in enhancing through-bond charge delocalization in conjugated 2D COFs, with Lieb lattice[15] being more favorable over Kagome lattice.[16] A complementary strategy for achieving through-space transport requires maximizing orbital interactions within the resulting layered framework structure through strategic choice of building blocks. Although several reports have taken advantage of π-stacking for designing COF-based materials with reasonable charge carrier mobilities (8.1 $cm^2\ V^{-1}\ s^{-1}$),[7c, 17] their bulk conductivities remained limited. We reasoned that by simultaneously capitalizing on both molecular design strategies of through-bond and through-space transport in a highly planar, two-dimensional, fully conjugated material based on a Lieb lattice may lead to the realization of a high intrinsic bulk electrical conductivity within a COF-based material.

This paper describes the development of a novel intrinsically conductive COF (**COF-DC-8**) through the condensation reaction between the highly planar conjugated building blocks: octaamino-derived nickelphthalocyanine (**NiOAPc**) and pyrenetetraone (**TOPyr**). The annulation of tetraketone and octaamine precursors to form pyrazine rings generates a fully aromatic conjugated framework structure with square apertures (**Scheme 1**). The utilization of the nickelphthalocyanine core was inspired by its application in the construction of conductive frameworks materials demonstrated by our group[18] and others,[3d, 19] as well as its affinity to small gaseous analytes.[20] The resulting fully conjugated 2D lattice with Lieb topology can maximize through-bond charge delocalization, while the stacking of the embedded metallophthalocyanine units confined within the rigid framework material can efficiently promote out-of-plane charge transfer. The bulk conductivity—which characterizes the weighted average of contributions from through-bond and through-space charge delocalization in polycrystalline **COF-DC-8**—reached 2.51×10^{-3} S/m, representing the highest bulk conductivity achieved within an intrinsically conductive COF.

Chemiresistive devices made from this conductive COF showed excellent responses and ultra-low limits of detection for gaseous analytes (1.5 min exposure-based LODs: 70 ppb for NH_3, 204 ppb for H_2S, 5 ppb for NO, and 16 ppb for NO_2). Increases in resistance towards reducing gases and decreases in resistance towards oxidizing gases were consistent with p-type semiconductive character of the COF. Spectroscopic characterization using electron paramagnetic resonance (EPR) and X-ray photoelectron spectroscopy (XPS) suggested that the chemiresistivite response of **COF-DC-8** originates from the combination of binding and charge transfer interactions between the analyte and the Ni-containing phthalocyanine component of the framework. The promising chemiresistive performance highlights the potential application of this modular class of materials in the fabrication of electronic devices and chemical sensors.

RESULTS AND DISCUSSION

Synthesis and Characterization. As drawn in **Scheme 1**, the condensation reaction performed in a mixed solvent of dimethylacetamide (DMAC) and *o*-diclorobenzene (DCB) in the presence of sulfuric acid for 10 days gave the desired **COF-DC-8** as a dark green powder (see **Section 2.2** in Supporting Information for details). Microwave heating significantly reduced the reaction time to 10 hours, albeit at the expense of slightly diminished crystallinity (entry 10 in **Table S1** and **Figure S6**). Efforts to optimize reaction conditions yielded several alternative approaches for accessing **COF-DC-8**, including the use of the aqueous solution of acetic acid in a mixed solvent system of DMAC and DCB (entry 14 in **Table S1** and **Figure S6**), and the use of NMP as the solvent in the presence of sulfuric acid or aqueous solution of acetic acid (entry 17, 18 in **Table S1** and **Figure S6**).

Fourier-transform infrared spectroscopy of **COF-DC-8** (**Figure S7**) showed the appearance of characteristic absorption bands of the phenazine system at 1518, 1431, and 1351 cm^{-1}, while absorption bands of C=O and $-NH_2$

groups from **NiOAPc** and **TOPyr** were absent, indicating the formation of phenazine linkages. XPS showed characteristic bands for the K-edge of carbon (285.9 eV) and nitrogen (398.6 eV) in C=N bond (**Figure S9**), indicating the presence of sp^2-hybridized nitrogen atoms. Elemental analysis showed that C:N:Ni ratios were consistent with theoretical values (**Table S2**), although the absolute percentages of C, N, and Ni were slightly lower than theoretical values. The discrepancy between the theoretical and observed values could be from the existence of unreacted C=O and NH_2 groups at sheet edges[7d] and the entrapment of small-molecule volatiles (acetone, H_2O, or DMAC) included in the pores, as suggested by XPS (**Figure S9** in **section 4**) and thermal gravimetric analysis (see **Figure S20** in **section 10**) analysis.

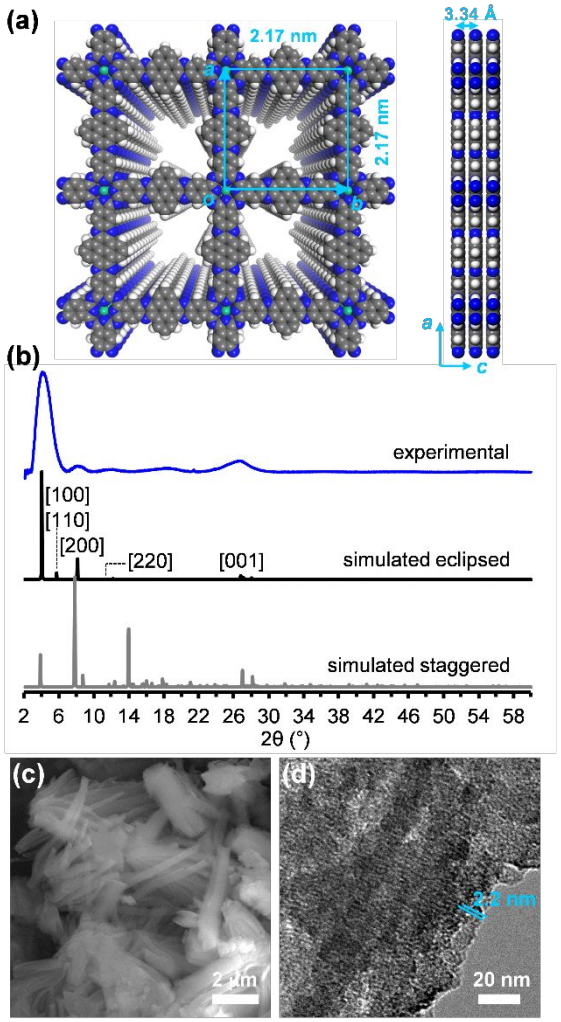

Figure 1. The structure and characterization of **COF-DC-8**. (a) Top and side view of the structure of **COF-DC-8** with 2 × 2 square grids in eclipsed stacking mode with a Lieb lattice. (b) Comparison of the simulated and experimental PXRD patterns of **COF-DC-8.** (c) SEM and (d) TEM of **COF-DC-8**.

Powder X-ray diffractometry (PXRD) further supported the formation of the desired framework formed under optimized reaction conditions (**Figure 1a-b**). Prominent peaks were observed at 2θ = 4.06°, 8.19°, 11.48°, 12.26°, and 26.65°, that were assigned to the [100], [200], [220], [300], and [001] facets, respectively (**Figure 1b**). Although PXRD displayed peak broadening which was possibly due to small crystallite size, the peak intensity and position were sufficient for confirming the framework structure and key cell parameters of **DC-COF-8**. The strong diffractions from the [100] and [200] facets indicated long-range order within the *ab* plane of the structure. The Ni-to-Ni distance on the side of the square, based on those two diffractions, was calculated to be 2.17 nm. The presence of the [001] facet at 26.65° suggested the structural ordering with a 3.34 Å separation of layers along the *c* axis perpendicular to the 2D sheets. These results were consistent with the structure optimized by DFT calculations with generalized gradient approximation functional (See **Section S6** in Supporting Information). The experimental PXRD was in good agreement with the simulated fully eclipsed AA-stacking model with a space group of P4/MMM characterized by cofacial stacking of metallophthalocyanine units in adjacent layers; in contrast, the staggered model with an offset by distances of *a*/2 and *b*/2 did not match the experimental PXRD pattern (**Figure 2b**, **Figure S11-S13**).

Scanning electron microscopy (SEM) revealed the presence of rod-shaped crystallites with lengths ranging from hundreds of nanometers to several micrometers and widths of hundreds of nanometers (**Figure 1c** and **Figure S17**). Transmission electron microscopy (HR-TEM) provided visualization of a layered morphology (**Figure 1d** and **Figure S18**). The presence of regular lines with a spacing of ~2.2 nm in TEM (**Figure 1d**) was consistent with the interatomic distances of the [100] plane inferred from PXRD and computational models. **COF-DC-8** exhibited reversible nitrogen sorption isotherm curves with a Brunauer-Emmett-Teller surface area of 360 m^2 g^{-1} (**Figure S19**). The pore-size distribution profile gave an accessible pore size of 1.7 nm. Thermogravimetric analysis showed excellent thermal stability of **COF-DC-8** with only a total 10% of mass loss upon heating to 510 °C (**Figure S20**). **COF-DC-8** maintained its crystallinity when treated with 12 M HCl and 14 M KOH for 24 h (**Figure S15**), confirming its chemically robust skeleton.

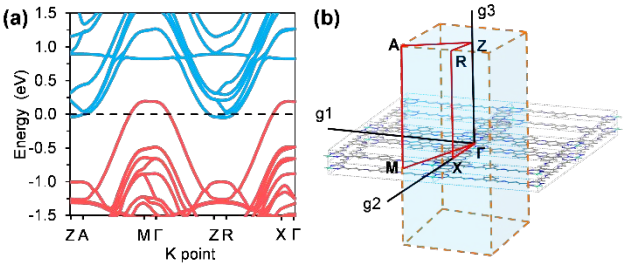

Figure 2. (a) Calculated electronic band structure of **COF-DC-8** and (b) the corresponding first Brillouin zone.

Electronic Properties. The electrical conductivity of **COF-DC-8** was measured using a four-point probe method

on a pressed pellet with a thickness of 1.0 mm. The bulk conductivity of **COF-DC-8** was determined to be 2.51×10^{-3} S/m at 298 K, which is several orders of magnitude higher than small-molecule nickel phthalocyanine[21] and a large number of other organic solids,[22] and is also significantly higher than many undoped conjugated polymers (10^{-4}–10^{-8} S/m)[23] and other pristine semi-conductive COFs.[7a, 8a, 8b, 8d, 9a] The Arrhenius fit to variable-temperature current measurements revealed an activation energy of 324 meV for the transport of charge carriers in **COF-DC-8 (Figure S22)**. Nearly a 10^3-fold improvement in conductivity was achieved by doping the COF with a gaseous stream of I_2 (~400 ppm in N_2) within 5 minutes of exposure at room temperature (**Figure S23**).

DFT calculations (see **Section S7** in Supporting information) were performed to gain insight into the electronic structure of the COF. The Dirac bands crossed the Fermi level in both A−M, Γ−Z, and R-X directions and exhibited wide band dispersions of more than 0.5 eV, suggesting the intrinsically conductive nature of **COF-DC-8**. The high symmetry points in the first Brillouin zone of **COF-DC-8** showed that the bands crossed the Fermi level through the out-of-plane directions (**Figure 2a**). In contrast, the in-plane direction, including Γ−M, Z−R, Γ−M and Z-A of the material, exhibited moderate band gaps ranging from 0.5−1.0 eV. These results suggested that the charge transport in **COF-DC-8** may be anisotropic and that a significant mechanism contributing to the bulk conductivity may be through pathways along the c-axis.[6d] The computed through space charge-transport property is consistent with those found in other phthalocyanine-[17b, 17c] and porphyrin-based COFs,[7c, 17d] that exhibited high carrier mobility along the direction of the stacking due to the formation of periodic π-columns. We hypothesize that the eclipsed stacking mode of **COF-DC-8** has the potential to amplify the alignment of the π-conjugated units and enhance the through-space metallophthalocyanine-to-metallophthalocyanine charge transport along the 2D stacks. Since the experimental validation of these calculations would require access to highly oriented nanosheets and nanowires of the COF, the polycrystalline material—which was the focus of this study—was not suitable for confirming these calculations experimentally.

Chemiresistivity of COF-DC-8. 2D COFs are highly appealing for the fabrication of electronic devices by virtue of their well-defined lattice with π functionality, large surface-to-volume ratio, and chemically robust skeleton. However, the poor to modest conductivity of existing 2D COFs has limited their use in electronic devices and other applications.[7a, 8a, 8c, 8d, 9a, 24] Given the good electrical conductivity and the ability of the built-in nickelphthalocyanine units to bind a wide range of analytes through coordination with the metal center,[18, 25] we tested the chemiresistive response of **COF-DC-8** towards a series of gases with different reducing and oxidizing abilities, including NH_3, H_2S, NO, and NO_2. These gases constitute well-known toxic pollutants and are also biological signaling molecules.[26] To make chemiresistive devices, a COF suspension was drop casted onto interdigitated electrodes, which gave devices with resistances in the range of kΩ (**Figure S24**). The devices were tested under a constant applied voltage of 1.0 V, and the current was monitored using a potentiostat.

Upon exposure to 40 ppm of NH_3 (balance gas N_2) for 30 min, **COF-DC-8** showed a normalized response ($-\Delta G/G_0$) of 39±1% (**Figure 3a, Figure S34a**). This positive change in resistance of **COF-DC-8** in response to NH_3, which typically serves as an electron donor, suggested that **COF-DC-8** behaved as a p-type semiconductor.[27] A response of 62±1% was observed to 40 ppm of H_2S (**Figure 3a, Figure S34a**). The higher response to H_2S, compared to NH_3, may be due to the stronger interaction between the material and H_2S. This response value was comparable with chemiresistive devices employing hexahydroxytriphenylene-based MOF[28] and metallophthalocyanine-based bimetallic MOF.[29] In contrast to the positive responses to NH_3 and H_2S, **COF-DC-8** exhibited negative response to both NO and NO_2 (**Figure 3b, Figure S34b**), which further reinforced the p-type character of **COF-DC-8**. The exposure of the COF to 40 ppm NO generated a high response of 3939± 317 % (**Figure 3c**). This remarkable response to

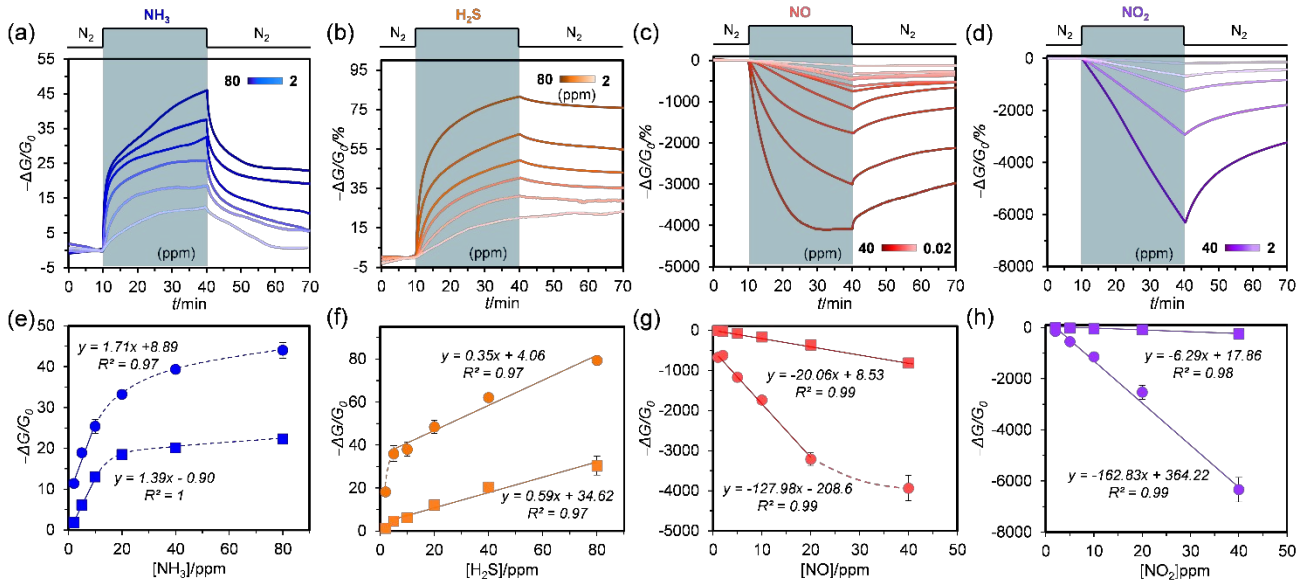

Figure 3. Chemiresistive responses of devices with integrated **COF-DC-8** to (a) NH_3, (b) H_2S, (c) NO, and (d) NO_2 under an applied voltage of 1.0 V and an atmosphere of dry nitrogen. Responses ($-\Delta G/G_0$) of **COF-DC-8** after 1.5 min (squares) and 30 min (circles) exposure versus concentration of (e) NH_3, (f) H_2S, (g) NO, and (h) NO_2.

NO was more than 10 times higher than that produced by triphenylene-based conductive MOFs.[28, 30] An even higher response of –6338± 479% was generated after the 30 min exposure of 40 ppm of NO_2 (**Figure 3d, Figure S34b**). This modulation of electrical conductivity of this COF by chemical doping with low-concentrations of small reactive gases has promising implications for developing advanced electronics where rectification of conductance is required.

Determination of LODs. Concentration-dependent studies (**Figure 3a-d**) enabled quantitative correlations between changes in response as a function of analyte concentration for **COF-DC-8**. Although the response values were distinguishable at [NH_3] =2–80 ppm, only a relatively narrow linear range of 2–10 ppm could be identified (**Figure 3e, Figure S27**). The LOD value for NH_3 determined from the response-concentration relationship in the linear range was 70 ppb based on 1.5 min exposure. Compared with NH_3, **COF-DC-8** showed a wider liner range of 5–80 ppm for H_2S that persisted across different exposure times ranging from 1.5 min to 30 min (**Figure 3f, Figure S29**). The LOD derived for H_2S detection was 204 ppb based on response values after 1.5 min exposure to the analyte. The calculated LOD values for both NH_3 and H_2S showed minimal dependence on exposure time with only slight changes observed for exposure time differences in the range of 1.5 min to 30 min (70-57 ppb for NH_3, 204-121 ppb for H_2S, see also **Table S4, S6**).

Excellent linear response-concentration relationships (R^2=0.98-0.99) were observed for NO and NO_2 at relatively wide concentration ranges of 0.02–40 ppm for NO and 2–40 ppm for NO_2(**Figure 3g**, **3h, Figure S31, Figure S33**). The striking sensitivity of **COF-DC-8** led to ultra-low LODs of 5 and 16 ppb for NO and NO_2, respectively, based on responses after 1.5 min exposure. Compared with those found for NH_3 and H_2S, significant exposure-time dependences were found for the LOD values of NO and NO_2 (**Table S8, S10**). Longer exposure times led to sub-ppb level of calculated LODs.

Recovery of Device Performance. Sensors characterized by high reversibility in response under repeated exposures to analyte are advantageous for their reusability. While dosimetric devices are highly irreversible when cycled through analyte exposures, they are advantageous to allow a historical record of total exposure events.[31] The response of **COF-DC-8** to NH_3 was partially reversible in the concentration range from 5 to 80 ppm (**Figure 3a, Table S3**). Full reversibility was observed when the concentration was below 2 ppm. Across the entire tested concentration range (2–80 ppm) for H_2S, only slight reversibility (5%-15%) was observed (**Figure 3b, Table S5**). The response to both NO and NO_2 showed partial reversibility (7%-33% for NO and 25%-45% for NO_2, **Figure 3c, 3d, Table S7, S9**). These observations demonstrated the dosimetric or quasi-dosimetric characteristics of **COF-DC-8** to H_2S, NO, and NO_2, in which the response was dependent on the dosing history.

In order to investigate the reusability of the devices, the analyte-exposed COF devices were reactivated by both thermal recovery and solvent recovery (**Section 12.2.6 in Supporting Information**). After solvent recovery by immersing in deionized water for 1 hour, the responses of devices were largely restored (108% for H_2S, 71% for NO, and 100% for NO_2). However, the devices were only partially restored (60% for H_2S, 14% for NO, and 17% for NO_2) their performance after thermal recovery by heating at 60 °C for 18 h under ~20 mTorr. These results were consistent with the previous report showing that, in metal–organic frameworks, washing was more efficient than heating for recovery of device performance.[28] The recovery tests suggested that analyte molecules bound by the material may be released

from the surface under aqueous conditions, thus restoring the sensing ability of the **COF-DC-8** device.

Analysis of Sensing Kinetics. The rate and magnitude of the chemiresistive response is usually governed by several factors, including the characteristics of the sensing apparatus,[32] the morphology and preferential orientation of the material,[33] and the electronic nature of the analyte.[4b] Analyzing the rate of response at the initial stage upon analyte exposure is a convenient technique that can allow rapid concentration-dependent measurements and convenient assessment of sensing kinetics when factors of the sensing apparatus and material characteristics are kept constant.[34]

Through the analysis of the initial rate of response, we found that **COF-DC-8** could differentiate certain analytes and their concentrations quantitatively within only 1 minute of initial analyte exposure (**Figure 4, Figure S36-S39**). Plotting the slope of initial response over the first 1 min of exposure versus the concentration of the four gases provided a linear relationship, which, in most cases, extended into much wider concentration ranges compared with those found in direct response-concentration analysis. This method provided a simple and fast analysis of the concentration of the four analytes.

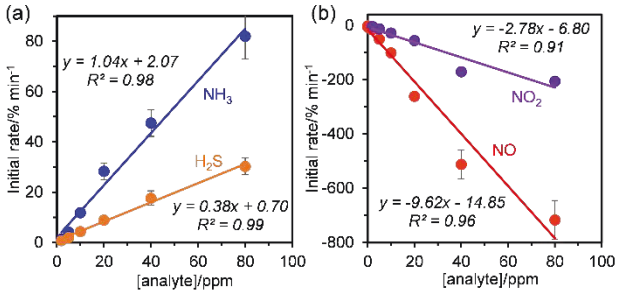

Figure 4. The initial rate of response as a function of concentration of (a) reducing gases NH_3 and H_2S and (b) oxidizing gases of NO and NO_2.

Each of the four gases showed distinct dynamics of response at wide concentration range. Under the concentration of 40 ppm, the rate of the initial response for NH_3 was 48±5% min^{-1}, while the initial response for H_2S showed a slower rate of 18±3% min^{-1} (**Figure S36, S37**). Compared with reducing gases NH_3 and H_2S, **COF-DC-8** showed much quicker response for NO and NO_2 at the initial state with rates at 513±53% min^{-1} and 171±8% min^{-1}, respectively (**Figure S38, S39**). This observation indicated that the initial rate of response was strongly dependent on type of the analyte-material interaction.[4]

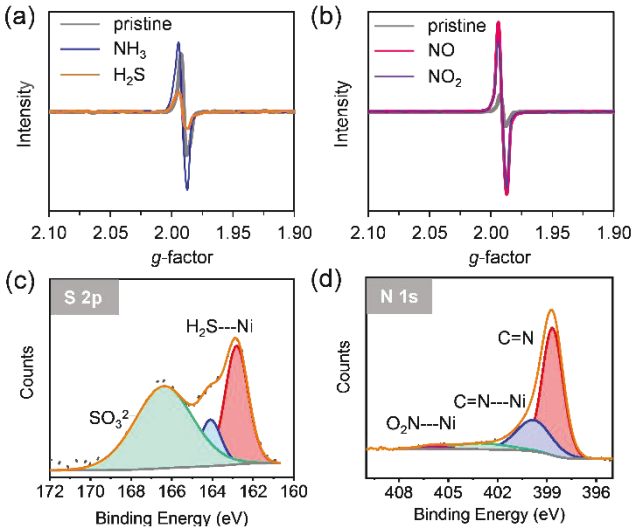

Figure 5. EPR spectrum of **COF-DC-8** before (dashed lines) and after dosing (solid lines) with (a) NH_3 and H_2S, and (b) NO and NO_2. For comparison, the intensity of the peaks has been normalized based on the peak intensity before analyte dosing. (c) XPS of S 2p range of **COF-DC-8** after H_2S exposure. (d) XPS of N 1s range of **COF-DC-8** after NO_2 exposure.

Sensing Mechanism. To investigate the sensing mechanism, spectroscopic analysis using EPR and XPS was performed. EPR analysis was carried out in the X-band at 77 K under N_2 atmosphere on COF samples before and after they were exposed to analytes (1% NH_3, H_2S, NO, and NO_2) for 1 hour. XPS analysis was carried out on analyte-exposed samples prepared by a similar procedure with those for EPR analysis, which were subsequently mounted on copper tape and analyzed under reduced pressure of ~10^{-7} Torr (see **Section 12.3** in Supporting information for details).

The EPR spectrum of pristine **COF-DC-8** showed a ligand centered radical at g = 1.99, which was likely due to the chemisorption of O_2 on the Ni center that induces unpaired radicals because of the charge transfer from the phthalocyanine ligand to O_2 molecule.[35] After NH_3 exposure, only a 15% intensity increase in EPR signal was observed (**Figure 5a**). No obvious change was detected on the XPS spectra of C 1s, N 1s, and Ni 2p (**Figure S41**) after NH_3 exposure. These results suggested that the interaction between NH_3 and **COF-DC-8** may be dominated by reversible and weak charge transfer interactions under tested conditions.[36]

After dosing **COF-DC-8** with H_2S, we observed a significant decrease in peak intensity of 70% in the EPR signal (**Figure 5a**). This observation may be consistent with the replacement of surface-bound O_2 by H_2S at the Ni centers. By XPS, clear emission lines at binding energies of 163.8 eV and 165.1 eV (**Figure 5c, Figure S42**) were detected, that were similar to S $2p_{1/2}$ and S $2p_{3/2}$ peaks found in metal sulfides,[37] which indicated the formation of Ni-S bond. Moreover, a prominent peak at a higher binding energy of 167.5 eV, consistent with the formation of sulphite species,

was also observed. This observation suggested that the Ni-bound H_2S may be further transformed into species with higher oxidation states, likely with the participation of surface adsorbed O_2 through a catalytic oxidation reaction.[37b] This type of irreversible transformation is consistent with the negligible recovery in response after H_2S exposure shown in **Figure 3b**.

After the exposure of the COF to oxidizing gases, prominent increases of 3.2- and 4.2-fold in the EPR signals were found after NO and NO_2 exposure, respectively (**Figure 5b**). No significant changes were observed for the XPS spectra of Ni 2p, indicating that the oxidation state of the Ni centers was not altered (**Figure S43, S44**). After NO dosing, a new component corresponding to N 1s appeared at the binding energy of 402.0 eV, which was absent in the pristine material. Based on the previous studies of NO adsorption on metal surfaces, this component was assigned as a Ni-bound NO species.[38] After NO_2 dosing, a weak, yet clear, peak was observed at the binding energy of 406.1 eV (**Figure 5d**). Through the comparison with spectra of NO_2 adsorbed on metallophthalocyanines[39] and metal oxides[40], this peak suggested the existence of NO_2 molecules which were likely coordinated to the Ni center. Taken together, the EPR and XPS results suggest that surface adsorption and charge transfer interactions between the analytes and nickelphthalocyanine component of the COF were critical to the observed chemiresistive properties of the COF.

CONCLUSION

In conclusion, we have designed and synthesized a novel intrinsically conductive **COF-DC-8** through the aromatic annulation between of 2,3,9,10,16,17,23,24-octa-aminophthalocyanine nickel(II) and pyrene-4,5,9,10-tetraone. The reaction between the tetraketone and octaamine allows the formation of pyrazine rings to generate a fully aromatic conjugated structure, and renders the construction of square apertures with a side length of 2.2 nm and excellent chemical and thermal stability. The bulk room temperature conductivity of **COF-DC-8** reached 2.51×10^{-3} S/m, which is the highest bulk conductivity achieved within an intrinsically conductive COF. Doping with I_2 can further increase the bulk conductivity by a factor of 10^3.

In the first implementation of a conductive COF as active material for chemiresistive devices, **COF-DC-8** showed excellent responses toward NH_3, H_2S, NO, and NO_2 with ultra-low limits of detection at ppb level, that is 70 ppb for NH_3, 204 ppb for H_2S, 5 ppb for NO, and 16 pb for NO_2 after only 1.5 min exposure to the analytes. These values are comparable to or superior to the most sensitive sensors based on conductive MOFs.[2] The sensing performance also significantly surpasses that of small-molecule metallophthalocyanines based chemiresistors,[25, 36a, 42] considering the high sensitivity and low driving voltage demand of **COF-DC-8**. We believe that this study forms the foundation for future design and development of highly conductive COFs and their high potential utility in chemical sensing, electronics, and electrical energy conversion and storage. Future studies focused on the exploration of templated epitaxial growth of the COF, the exfoliation of its thin layer forms, as well as examining the influence of the central element in the phthalocyanine component on structure-property relationships, will be required for enhanced understanding of this COF system and the fabrication of highly modular advanced electronic devices and sensing arrays.

ASSOCIATED CONTENT

Supporting Information

The Supporting Information is available free of charge on the ACS Publications website.

Synthetic details, characterization, and conductivity measurements, and sensing experiments (PDF).

AUTHOR INFORMATION

Corresponding Author

Katherine.A.Mirica@dartmouth.edu

Notes

The authors declare no competing financial interests.

ACKNOWLEDGMENT

K.A.M. acknowledges support from startup funds provided by Dartmouth College, from the Walter and Constance Burke Research Initiation Award, Army Research Office Young Investigator Program Grant No. W911NF-17-1-0398, National Science Foundation EPSCoR award (#1757371), Sloan Research Fellowship (FG-2018-10561),3M Non-Tenured Faculty Award, and Arthur L. Irving Institute for Energy and Society at Dartmouth. The authors thank the University Instrumentation Center at the University of New Hampshire (Durham, NH) for the access to XPS, Mr. Maciej M. Kmiec for the assistance with EPR, and Mr. Chang Liu for the assistance with TGA.

REFERENCES

1. Zeng, M.; Xiao, Y.; Liu, J.; Yang, K.; Fu, L. Exploring Two-Dimensional Materials toward the Next-Generation Circuits: From Monomer Design to Assembly Control. *Chem. Rev.* **2018,** *118*, 6236.

2. (a) Sheberla, D.; Bachman, J. C.; Elias, J. S.; Sun, C. J.; Shao-Horn, Y.; Dincă, M. Conductive Mof Electrodes for Stable Supercapacitors with High Areal Capacitance. *Nat. Mater.* **2016,** *16*, 220; (b) Feng, D.; Lei, T.; Lukatskaya, M. R.; Park, J.; Huang, Z.; Lee, M.; Shaw, L.; Chen, S.; Yakovenko, A. A.; Kulkarni, A.; Xiao, J.; Fredrickson, K.; Tok, J. B.; Zou, X.; Cui, Y.; Bao, Z. Robust and Conductive Two-Dimensional Metal−Organic Frameworks with Exceptionally High Volumetric and Areal Capacitance. *Nat. Energy.* **2018,** *3*, 30; (c) Park, J.; Lee, M.; Feng, D.; Huang, Z.; Hinckley, A. C.; Yakovenko, A.; Zou, X.; Cui, Y.; Bao, Z. Stabilization of Hexaaminobenzene in a 2D Conductive Metal–Organic Framework for High Power Sodium Storage. *J. Am. Chem. Soc.* **2018,** *140*, 10315.

3. (a) Dong, R.; Pfeffermann, M.; Liang, H.; Zheng, Z.; Zhu, X.; Zhang, J.; Feng, X. Large-Area, Free-Standing, Two-Dimensional Supramolecular Polymer Single-Layer Sheets for Highly Efficient Electrocatalytic Hydrogen Evolution. *Angew. Chem. Int. Ed.* **2015,** *54*, 12058; (b) Zhang, P.; Hou, X.; Liu, L.; Mi, J.; Dong, M. Two-Dimensional π-Conjugated Metal Bis(Dithiolene) Complex Nanosheets as Selective Catalysts for Oxygen Reduction Reaction. *J. Phys. Chem. C* **2015,** *119*, 28028; (c) Miner, E. M.; Fukushima, T.; Sheberla, D.; Sun, L.; Surendranath, Y.; Dincă, M. Electrochemical Oxygen Reduction Catalysed by Ni_3(Hexaiminotriphenylene)$_2$. *Nat Commun* **2016,** *7*, 10942; (d) Jia, H.; Yao, Y.; Zhao, J.; Gao, Y.; Luo, Z.; Du, P. A Novel Two-Dimensional Nickel Phthalocyanine-Based Metal–Organic Framework for Highly Efficient Water Oxidation Catalysis. *J. Mater. Chem. A* **2018,** *6*, 1188.

4. (a) Varghese, S.; Varghese, S.; Swaminathan, S.; Singh, K.; Mittal, V. Two-Dimensional Materials for Sensing: Graphene and Beyond. *Electronics* **2015,** *4*, 651; (b) Meng, Z.; Stolz, R. M.; Mendecki, L.; Mirica, K. A. Electrically-Transduced Chemical Sensors Based on Two-Dimensional Nanomaterials. *Chem. Rev.* **2019**, *119*, 478.

5. (a) Hendon, C. H.; Rieth, A. J.; Korzyński, M. D.; Dincă, M. Grand Challenges and Future Opportunities for Metal–Organic Frameworks. *ACS Cent. Sci.* **2017,** *3*, 554; (b) Sun, L.; Campbell, M. G.; Dincă, M. Electrically Conductive Porous Metal–Organic Frameworks. *Angew. Chem. Int. Ed.* **2016,** *55*, 3566; (c) Ko, M.; Mendecki, L.; Mirica, K. A. Conductive Two-Dimensional Metal–Organic Frameworks as Multifunctional Materials. *Chem. Commun.* **2018,** *54*, 7873; (d) Hmadeh, M.; Lu, Z.; Liu, Z.; Gándara, F.; Furukawa, H.; Wan, S.; Augustyn, V.; Chang, R.; Liao, L.; Zhou, F.; Perre, E.; Ozolins, V.; Suenaga, K.; Duan, X.; Dunn, B.; Yamamto, Y.; Terasaki, O.; Yaghi, O. M. New Porous Crystals of Extended Metal-Catecholates. *Chem. Mater.* **2012,** *24*, 3511.

6. (a) Huang, X.; Zhang, S.; Liu, L.; Yu, L.; Chen, G.; Xu, W.; Zhu, D. Superconductivity in a Copper(II)-Based Coordination Polymer with Perfect Kagome Structure. *Angew. Chem. Int. Ed.* **2018,** *57*, 146; (b) Huang, X.; Sheng, P.; Tu, Z.; Zhang, F.; Wang, J.; Geng, H.; Zou, Y.; Di, C. A.; Yi, Y.; Sun, Y.; Xu, W.; Zhu, D. A Two-Dimensional Pi-D Conjugated Coordination Polymer with Extremely High Electrical Conductivity and Ambipolar Transport Behaviour. *Nat. Commun.* **2015,** *6*, 7408; (c) Dou, J. H.; Sun, L.; Ge, Y.; Li, W.; Hendon, C. H.; Li, J.; Gul, S.; Yano, J.; Stach, E. A.; Dincă, M. Signature of Metallic Behavior in the Metal–Organic Frameworks M_3(Hexaiminobenzene)$_2$ (M = Ni, Cu). *J. Am. Chem. Soc.* **2017,** *139*, 13608; (d) Clough, A. J.; Skelton, J. M.; Downes, C. A.; de la Rosa, A. A.; Yoo, J. W.; Walsh, A.; Melot, B. C.; Marinescu, S. C. Metallic Conductivity in a Two-Dimensional Cobalt Dithiolene Metal–Organic Framework. *J. Am. Chem. Soc.* **2017,** *139*, 10863.

7. (a) Yang, H.; Zhang, S.; Han, L.; Zhang, Z.; Xue, Z.; Gao, J.; Li, Y.; Huang, C.; Yi, Y.; Liu, H.; Li, Y. High Conductive Two-Dimensional Covalent Organic Framework for Lithium Storage with Large Capacity. *ACS Appl. Mater. Interfaces* **2016,** *8*, 5366; (b) Gu, C.; Huang, N.; Chen, Y.; Qin, L.; Xu, H.; Zhang, S.; Li, F.; Ma, Y.; Jiang, D. Π-Conjugated Microporous Polymer Films: Designed Synthesis, Conducting Properties, and Photoenergy Conversions. *Angew. Chem.* **2015,** *127*, 13798; (c) Wan, S.; Gándara, F.; Asano, A.; Furukawa, H.; Saeki, A.; Dey, S. K.; Liao, L.; Ambrogio, M. W.; Botros, Y. Y.; Duan, X.; Seki, S.; Stoddart, J. F.; Yaghi, O. M. Covalent Organic Frameworks with High Charge Carrier Mobility. *Chem. Mater.* **2011,** *23*, 4094; (d) Mahmood, J.; Lee, E. K.; Jung, M.; Shin, D.; Jeon, I. Y.; Jung, S. M.; Choi, H. J.; Seo, J. M.; Bae, S. Y.; Sohn, S. D.; Park, N.; Oh, J. H.; Shin, H. J.; Baek, J. B. Nitrogenated Holey Two-Dimensional Structures. *Nat. Commun.* **2015,** *6*, 6486; (e) Guo, J.; Xu, Y.; Jin, S.; Chen, L.; Kaji, T.; Honsho, Y.; Addicoat, M. A.; Kim, J.; Saeki, A.; Ihee, H.; Seki, S.; Irle, S.; Hiramoto, M.; Gao, J.; Jiang, D. Conjugated Organic Framework with Three-Dimensionally Ordered Stable Structure and Delocalized Pi Clouds. *Nat. Commun.* **2013,** *4*, 2736.

8. (a) Jin, E.; Asada, M.; Xu, Q.; Dalapati, S.; Addicoat, M. A.; Brady, M. A.; Xu, H.; Nakamura, T.; Heine, T.; Chen, Q.; Jiang, D. Two-Dimensional sp^2 Carbon-Conjugated Covalent Organic Frameworks. *Science* **2017,** *357*, 673; (b) Cai, S.-L.; Zhang, Y.-B.; Pun, A. B.; He, B.; Yang, J.; Toma, F. M.; Sharp, I. D.; Yaghi, O. M.; Fan, J.; Zheng, S.-R.; Zhang, W.-G.; Liu, Y. Tunable Electrical Conductivity in Oriented Thin Films of Tetrathiafulvalene-Based Covalent Organic Framework. *Chem. Sci.* **2014,** *5*, 4693; (c) Mulzer, C. R.; Shen, L.; Bisbey, R. P.; McKone, J. R.; Zhang, N.; Abruna, H. D.; Dichtel, W. R. Superior Charge Storage and Power Density of a Conducting Polymer-Modified Covalent Organic Framework. *ACS Cent. Sci.* **2016,** *2*, 667; (d) Wu, Y.; Yan, D.; Zhang, Z.; Matsushita, M. M.; Awaga, K. Electron Highways into Nanochannels of Covalent Organic Frameworks for High Electrical Conductivity and Energy Storage. *ACS Appl. Mater. Interfaces* **2019,** *11*, 7661; (e) Bertrand, G. H.; Michaelis, V. K.; Ong, T. C.; Griffin, R. G.; Dincă, M. Thiophene-Based Covalent Organic Frameworks. *Proc. Natl. Acad. Sci. U. S. A.* **2013,** *110*, 4923.

9. (a) Medina, D. D.; Sick, T.; Bein, T. Photoactive and Conducting Covalent Organic Frameworks. *Adv Energy Mater* **2017,** *7*, 1700387; (b) Wang, L.; Zeng, C.; Xu, H.; Yin, P.; Chen, D.; Deng, J.; Li, M.; Zheng, N.; Gu, C.; Ma, Y. A Highly Soluble, Crystalline Covalent Organic Framework Compatible with Device Implementation. *Chem Sci* **2019,** *10*, 1023.

10. (a) Swager, T. M. 50th Anniversary Perspective: Conducting/Semiconducting Conjugated Polymers. A Personal Perspective on the Past and the Future. *Macromolecules* **2017,** *50*, 4867; (b) Kertesz, M.; Choi, C. H.; Yang, S. Conjugated Polymers and Aromaticity. *Chem. Rev.* **2005,** *105*, 3448.

11. (a) Ferraris, J.; Cowan, D. O.; Walatka, V.; Perlstein, J. H. Electron Transfer in a New Highly Conducting Donor-Acceptor Complex. *J. Am. Chem. Soc.* **1973,** *95*, 948; (b) Petersen, J. L.; Schramm, C. S.; Stojakovic, D. R.; Hoffman, B. M.; Marks, T. J. A New Class of Highly Conductive Molecular Solids: The Partially Oxidized Phthalocyanines. *J. Am. Chem. Soc.* **1977,** *99*, 286; (c) Hush, N. S. An Overview of the First Half-Century of Molecular Electronics. *Ann. N. Y. Acad. Sci.* **2003,** *1006*, 1.

12. Givaja, G.; Amo-Ochoa, P.; Gomez-Garcia, C. J.; Zamora,

F. Electrical Conductive Coordination Polymers. *Chem. Soc. Rev.* **2012,** *41*, 115.

13. (a) Sirringhaus, H.; Brown, P. J.; Friend, R. H.; Nielsen, M. M.; Bechgaard, K.; Langeveld-Voss, B. M. W.; Spiering, A. J. H.; Janssen, R. A. J.; Meijer, E. W.; Herwig, P.; de Leeuw, D. M. Two-Dimensional Charge Transport in Self-Organized, High-Mobility Conjugated Polymers. *Nature* **1999,** *401*, 685; (b) McCulloch, I.; Heeney, M.; Bailey, C.; Genevicius, K.; Macdonald, I.; Shkunov, M.; Sparrowe, D.; Tierney, S.; Wagner, R.; Zhang, W.; Chabinyc, M. L.; Kline, R. J.; McGehee, M. D.; Toney, M. F. Liquid-Crystalline Semiconducting Polymers with High Charge-Carrier Mobility. *Nat. Mater.* **2006,** *5*, 328; (c) Gutzler, R.; Perepichka, D. F. Pi-Electron Conjugation in Two Dimensions. *J. Am. Chem. Soc.* **2013,** *135*, 16585.

14. Abel, M.; Clair, S.; Ourdjini, O.; Mossoyan, M.; Porte, L. Single Layer of Polymeric Fe-Phthalocyanine: An Organometallic Sheet on Metal and Thin Insulating Film. *J. Am. Chem. Soc.* **2011,** *133*, 1203.

15. Slot, M. R.; Gardenier, T. S.; Jacobse, P. H.; van Miert, G. C. P.; Kempkes, S. N.; Zevenhuizen, S. J. M.; Smith, C. M.; Vanmaekelbergh, D.; Swart, I. Experimental Realization and Characterization of an Electronic Lieb Lattice. *Nat. Phys.* **2017,** *13*, 672.

16. Thomas, S.; Li, H.; Zhong, C.; Matsumoto, M.; Dichtel, W. R.; Bredas, J.-L. Electronic Structure of Two-Dimensional Π-Conjugated Covalent Organic Frameworks. *Chem. Mater.* **2019,** *31*, 3051.

17. (a) Ding, X.; Chen, L.; Honsho, Y.; Feng, X.; Saengsawang, O.; Guo, J.; Saeki, A.; Seki, S.; Irle, S.; Nagase, S.; Parasuk, V.; Jiang, D. An n-Channel Two-Dimensional Covalent Organic Framework. *J. Am. Chem. Soc.* **2011,** *133*, 14510; (b) Jin, S.; Ding, X.; Feng, X.; Supur, M.; Furukawa, K.; Takahashi, S.; Addicoat, M.; El-Khouly, M. E.; Nakamura, T.; Irle, S.; Fukuzumi, S.; Nagai, A.; Jiang, D. Charge Dynamics in a Donor-Acceptor Covalent Organic Framework with Periodically Ordered Bicontinuous Heterojunctions. *Angew. Chem. Int. Ed.* **2013,** *52*, 2017; (c) Ding, X.; Feng, X.; Saeki, A.; Seki, S.; Nagai, A.; Jiang, D. Conducting Metallophthalocyanine 2D Covalent Organic Frameworks: The Role of Central Metals in Controlling Pi-Electronic Functions. *Chem. Commun.* **2012,** *48*, 8952; (d) Feng, X.; Liu, L.; Honsho, Y.; Saeki, A.; Seki, S.; Irle, S.; Dong, Y.; Nagai, A.; Jiang, D. High-Rate Charge-Carrier Transport in Porphyrin Covalent Organic Frameworks: Switching from Hole to Electron to Ambipolar Conduction. *Angew. Chem. Int. Ed.* **2012,** *51*, 2618; (e) Yang, L.; Wei, D.-C. Semiconducting Covalent Organic Frameworks: A Type of Two-Dimensional Conducting Polymers. *Chin. Chem. Lett.* **2016,** *27*, 1395; (f) Ding, X. S.; Guo, J.; Feng, X. A.; Honsho, Y.; Guo, J. D.; Seki, S.; Maitarad, P.; Saeki, A.; Nagase, S.; Jiang, D. L. Synthesis of Metallophthalocyanine Covalent Organic Frameworks That Exhibit High Carrier Mobility and Photoconductivity. *Angew. Chem. Int. Ed.* **2011,** *50*, 1289.

18. Meng, Z.; Aykanat, A.; Mirica, K. A. Welding Metallophthalocyanines into Bimetallic Molecular Meshes for Ultrasensitive, Low-Power Chemiresistive Detection of Gases. *J. Am. Chem. Soc.* **2019,** *141*, 2046.

19. Nagatomi, H.; Yanai, N.; Yamada, T.; Shiraishi, K.; Kimizuka, N. Synthesis and Electric Properties of a Two-Dimensional Metal–Organic Framework Based on Phthalocyanine. *Chem. Eur. J.* **2018,** *24*, 1806.

20. Kutzler, F. W.; Barger, W. R.; Snow, A. W.; Wohltjen, H. An Investigation of Conductivity in Metal-Substituted Phthalocyanine Langmuir-Blodgett Films. *Thin Solid Films* **1987,** *155*, 1.

21. (a) Claessens, C. G.; Hahn, U.; Torres, T. Phthalocyanines: From Outstanding Electronic Properties to Emerging Applications. *Chem. Rec.* **2008,** *8*, 75; (b) Assour, J. M.; Harrison, S. E. Electrical Conductivity of Metal-Free and Copper Phthalocyanine Crystals. *J. Phys. Chem. Solids* **1965,** *26*, 670.

22. (a) Zhang, Y.; Duan, Y.; Song, L.; Zheng, D.; Zhang, M.; Zhao, G. Charge-Transfer Mobility and Electrical Conductivity of Pani as Conjugated Organic Semiconductors. *J. Chem. Phys.* **2017,** *147*, 114905; (b) Jacobs, I. E.; Moule, A. J. Controlling Molecular Doping in Organic Semiconductors. *Adv. Mater.* **2017,** *29*, 1703063.

23. Le, T.-H.; Kim, Y.; Yoon, H. Electrical and Electrochemical Properties of Conducting Polymers. *Polymers* **2017,** *9*, 150.

24. DeBlase, C. R.; Hernandez-Burgos, K.; Silberstein, K. E.; Rodriguez-Calero, G. G.; Bisbey, R. P.; Abruna, H. D.; Dichtel, W. R. Rapid and Efficient Redox Processes within 2D Covalent Organic Framework Thin Films. *ACS Nano* **2015,** *9*, 3178.

25. (a) Mukherjee, D.; Manjunatha, R.; Sampath, S.; Ray, A. K., Phthalocyanines as Sensitive Materials for Chemical Sensors. In *Materials for Chemical Sensing*, Springer: 2017; pp 165; (b) Zhou, R.; Josse, F.; Göpel, W.; Öztürk, Z. Z.; Bekaroğlu, Ö. Phthalocyanines as Sensitive Materials for Chemical Sensors. *Appl. Organomet. Chem.* **1996,** *10*, 557.

26. (a) Calvert, J. G.; Lazrus, A.; Kok, G. L.; Heikes, B. G.; Walega, J. G.; Lind, J.; Cantrell, C. A. Chemical Mechanisms of Acid Generation in the Troposphere. *Nature* **1985,** *317*, 27; (b) Kant, R.; Bhattacharya, S., Sensors for Air Monitoring. In *Environmental, Chemical and Medical Sensors*, 2018; pp 9; (c) Mustafa, A. K.; Gadalla, M. M.; Snyder, S. H. Signaling by Gasotransmitters. *Sci Signal* **2009,** *2*, re2; (d) Edelson, S. Sending Ammonia Signals. *Science-Business eXchange* **2010,** *3*, 578; (e) Singer, M. A. Ammonia Functions as a Regulatory Molecule to Mediate Adjustments in Glomerular Filtration Rate in Response to Changes in Metabolic Rate. *Med. Hypotheses* **2001,** *57*, 740.

27. Jiang, J. *Functional Phthalocyanine Molecular Materials*. Springer: 2010.

28. Smith, M. K.; Mirica, K. A. Self-Organized Frameworks on Textiles (SOFT): Conductive Fabrics for Simultaneous Sensing, Capture, and Filtration of Gases. *J. Am. Chem. Soc.* **2017,** *139*, 16759.

29. Meng, Z.; Aykanat, A.; Mirica, K. A. Welding Metallophthalocyanines into Bimetallic Molecular Meshes for Ultrasensitive, Low-Power Chemiresistive Detection of Gases. *J. Am. Chem. Soc.* **2019,** *141*, 2046.

30. (a) Smith, M. K.; Jensen, K. E.; Pivak, P. A.; Mirica, K. A. Direct Self-Assembly of Conductive Nanorods of Metal–Organic Frameworks into Chemiresistive Devices on Shrinkable Polymer Films. *Chem. Mater.* **2016,** *28*, 5264; (b) Ko, M.; Aykanat, A.; Smith, M. K.; Mirica, K. A. Drawing Sensors

with Ball-Milled Blends of Metal–Organic Frameworks and Graphite. *Sensors* **2017,** *17*, 2192.

31. (a) Bănică, F.-G. *Chemical Sensors and Biosensors*. John Wiley & Sons, 2012; (b) Erdely, A.; Dahm, M.; Chen, B. T.; Zeidler-Erdely, P. C.; Fernback, J. E.; Birch, M. E.; Evans, D. E.; Kashon, M. L.; Deddens, J. A.; Hulderman, T.; Bilgesu, S. A.; Battelli, L.; Schwegler-Berry, D.; Leonard, H. D.; McKinney, W.; Frazer, D. G.; Antonini, J. M.; Porter, D. W.; Castranova, V.; Schubauer-Berigan, M. K. Carbon Nanotube Dosimetry: From Workplace Exposure Assessment to Inhalation Toxicology. *Part. Fibre Toxicol.* **2013,** *10*, 53.

32. Reghu, A.; LeGore, L. J.; Vetelino, J. F.; Lad, R. J.; Frederick, B. G. Distinguishing Bulk Conduction from Band Bending Transduction Mechanisms in Chemiresistive Metal Oxide Gas Sensors. *J. Phys. Chem. C* **2018,** *122*, 10607.

33. (a) Hoppe, B.; Hindricks, K. D. J.; Warwas, D. P.; Schulze, H. A.; Mohmeyer, A.; Pinkvos, T. J.; Zailskas, S.; Krey, M. R.; Belke, C.; König, S.; Fröba, M.; Haug, R. J.; Behrens, P. Graphene-Like Metal–Organic Frameworks: Morphology Control, Optimization of Thin Film Electrical Conductivity and Fast Sensing Applications. *CrystEngComm* **2018,** *20*, 6458; (b) Gargiulo, V.; Alfano, B.; Di Capua, R.; Alfé, M.; Vorokhta, M.; Polichetti, T.; Massera, E.; Miglietta, M. L.; Schiattarella, C.; Di Francia, G. Graphene-Like Layers as Promising Chemiresistive Sensing Material for Detection of Alcohols at Low Concentration. *J. Appl. Phys.* **2018,** *123,* 024503; (c) Donarelli, M.; Ottaviano, L.; Giancaterini, L.; Fioravanti, G.; Perrozzi, F.; Cantalini, C. Exfoliated Black Phosphorus Gas Sensing Properties at Room Temperature. *2D Mater.* **2016,** *3*, 025002.

34. (a) Riedel, K.; Renneberg, R.; Khn, M.; Scheller, F. A Fast Estimation of Biochemical Oxygen Demand Using Microbial Sensors. *Appl. Microbiol. Biotechnol.* **1988,** *28*, 316; (b) Tan, T. C.; Li, F.; Neoh, K. G. Measurement of Bod by Initial Rate of Response of a Microbial Sensor. *Sensors Actuators B: Chem.* **1993,** *10*, 137.

35. (a) Bohrer, F. I.; Colesniuc, C. N.; Park, J.; Ruidiaz, M. E.; Schuller, I. K.; Kummel, A. C.; Trogler, W. C. Comparative Gas Sensing in Cobalt, Nickel, Copper, Zinc, and Metal-Free Phthalocyanine Chemiresistors. *J. Am. Chem. Soc.* **2009,** *131*, 478; (b) Bohrer, F. I.; Sharoni, A.; Colesniuc, C.; Park, J.; Schuller, I. K.; Kummel, A. C.; Trogler, W. C. Gas Sensing Mechanism in Chemiresistive Cobalt and Metal-Free Phthalocyanine Thin Films. *J. Am. Chem. Soc.* **2007,** *129*, 5640.

36. (a) Collins, R. A.; Mohammed, K. A. Gas Sensitivity of Some Metal Phthalocyanines. *J. Phys. D: Appl. Phys.* **1988,** *21*, 154; (b) Zou, D.; Zhao, W.; Cui, B.; Li, D.; Liu, D. Adsorption of Gas Molecules on a Manganese Phthalocyanine Molecular Device and Its Possibility as a Gas Sensor. *Phys. Chem. Chem. Phys.* **2018,** *20*, 2048; (c) Klyamer, D. D.; Sukhikh, A. S.; Krasnov, P. O.; Gromilov, S. A.; Morozova, N. B.; Basova, T. V. Thin Films of Tetrafluorosubstituted Cobalt Phthalocyanine: Structure and Sensor Properties. *Appl. Surf. Sci.* **2016,** *372*, 79.

37. (a) Ko, T. H.; Chu, H. Spectroscopic Study on Sorption of Hydrogen Sulfide by Means of Red Soil. *Spectrochim. Acta. A Mol. Biomol. Spectrosc.* **2005,** *61*, 2253; (b) Galtayries, A.; Bonnelle, J. P. XPS and ISS Studies on the Interaction of H_2S with Polycrystalline Cu, Cu_2O and CuO Surfaces. *Surf. Interface Anal.* **1995,** *23*, 171; (c) Zhang, X.; Dou, G. Y.; Wang, Z.; Li, L.; Wang, Y. F.; Wang, H. L.; Hao, Z. P. Selective Catalytic Oxidation of H_2S over Iron Oxide Supported on Alumina-Intercalated Laponite Clay Catalysts. *J. Hazard. Mater.* **2013,** *260*, 104.

38. (a) Herranz, T.; Deng, X.; Cabot, A.; Liu, Z.; Salmeron, M. In Situ Xps Study of the Adsorption and Reactions of NO and O_2 on Gold Nanoparticles Deposited on TiO_2 and SiO_2. *J. Catal.* **2011,** *283*, 119; (b) Venezia, A. M.; Liotta, L. F.; Deganello, G.; Terreros, P.; Peña, M. A.; Fierro, J. L. G. IR and XPS Study of NO and CO Interaction with Palladium Catalysts Supported on Aluminosilicates. *Langmuir* **1999,** *15*, 1176; (c) Bukhtiyarov, A. V.; Kvon, R. I.; Nartova, A. V.; Bukhtiyarov, V. I. An XPS and STM Study of the Size Effect in NO Adsorption on Gold Nanoparticles. *Russ. Chem. Bull.* **2012,** *60*, 1977.

39. (a) Mrwa, A.; Friedrich, M.; Hofmann, A.; Zahn, D. R. T. Response of Lead Phthalocyanine to High NO_2 Concentration. *Sensors Actuators B: Chem.* **1995,** *25*, 596; (b) Mockert, H.; Graf, K.; Schmeisser, D.; Göpel, W.; Ahmad, Z. A.; Archer, P. B. M.; Chadwick, A. V.; Wright, J. D. Characterization of Gas-Sensitive Lead Phthalocyanine Film Surfaces by X-Ray Photoelectron Spectroscopy. *Sensors Actuators B: Chem.* **1990,** *2*, 133.

40. Baltrusaitis, J.; Jayaweera, P. M.; Grassian, V. H. XPS Study of Nitrogen Dioxide Adsorption on Metal Oxide Particle Surfaces under Different Environmental Conditions. *Phys. Chem. Chem. Phys.* **2009,** *11*, 8295.

41. (a) Campbell, M. G.; Sheberla, D.; Liu, S. F.; Swager, T. M.; Dincă, M. Cu_3(Hexaiminotriphenylene)$_2$: An Electrically Conductive 2D Metal–Organic Framework for Chemiresistive Sensing. *Angew. Chem. Int. Ed.* **2015,** *54*, 4349; (b) Yao, M.-S.; Lv, X.-J.; Fu, Z.-H.; Li, W.-H.; Deng, W.-H.; Wu, G.-D.; Xu, G. Layer-by-Layer Assembled Conductive Metal–Organic Framework Nanofilms for Room-Temperature Chemiresistive Sensing. *Angew. Chem. Int. Ed.* **2017,** *129*, 16737; (c) Campbell, M. G.; Liu, S. F.; Swager, T. M.; Dincă, M. Chemiresistive Sensor Arrays from Conductive 2D Metal–Organic Frameworks. *J. Am. Chem. Soc.* **2015,** *137*, 13780.

42. (a) Temofonte, T. A.; Schoch, K. F. Phthalocyanine Semiconductor Sensors for Room-Temperature ppb Level Detection of Toxic Gases. *J. Appl. Phys.* **1989,** *65*, 1350; (b) Li, X.; Jiang, Y.; Xie, G.; Tai, H.; Sun, P.; Zhang, B. Copper Phthalocyanine Thin Film Transistors for Hydrogen Sulfide Detection. *Sensors Actuators B: Chem.* **2013,** *176*, 1191; (c) Ho, K.-C.; Chen, C.-M.; Liao, J.-Y. Enhancing Chemiresistor-Type NO Gas-Sensing Properties Using Ethanol-Treated Lead Phthalocyanine Thin Films. *Sensors Actuators B: Chem.* **2005,** *108*, 418.

Table of Contents artwork here